



Exact frequency and phase control of a terahertz laser

RESHMA A. MOHANDAS,^{1,3} LALITHA PONNAMPALAM,²  LIANHE LI,¹  PAUL DEAN,¹ 
ALWYN J. SEEDS,² EDMUND H. LINFIELD,¹  A. GILES DAVIES,¹  AND JOSHUA R. FREEMAN^{1,4} 

¹School of Electronic and Electrical Engineering, University of Leeds, Leeds, LS2 9JT, UK

²School of Electronic and Electrical Engineering, University College London, London, WC1E 7JE, UK

³e-mail: eenra@leeds.ac.uk

⁴e-mail: J.R.Freeman@leeds.ac.uk

Received 24 April 2020; revised 9 July 2020; accepted 10 July 2020 (Doc. ID 395941); published 3 September 2020

The accuracy of high-resolution spectroscopy depends critically on the stability, frequency control, and traceability available from laser sources. In this work, we report exact tunable frequency synthesis and phase control of a terahertz laser. The terahertz laser is locked by a terahertz injection phase lock loop for the first time, with the terahertz signal generated by heterodyning selected lines from an all-fiber infrared frequency comb generator in an ultrafast photodetector. The comb line frequency separation is exactly determined by a Global Positioning System-locked microwave frequency synthesizer, providing traceability of the terahertz laser frequency to primary standards. The locking technique reduced the heterodyne linewidth of the terahertz laser to a measurement instrument-limited linewidth of <1 Hz, robust against short- and long-term environmental fluctuations. The terahertz laser frequency can be tuned in increments determined only by the microwave synthesizer resolution, and the phase of the laser, relative to the reference, is independently and precisely controlled within a range $\pm 0.3\pi$. These findings are expected to enable applications in phase-resolved high-precision terahertz gas spectroscopy and radiometry.

Published by The Optical Society under the terms of the [Creative Commons Attribution 4.0 License](https://creativecommons.org/licenses/by/4.0/). Further distribution of this work must maintain attribution to the author(s) and the published article's title, journal citation, and DOI.

<https://doi.org/10.1364/OPTICA.395941>

1. INTRODUCTION

An ideal single-frequency laser produces an electromagnetic wave that is defined by three values: its amplitude, frequency, and phase. Since the invention of the laser [1] there has been a huge effort devoted both to stabilize these parameters to ensure that they remain constant over time and to control them with high precision. The highly stable and precise laser sources that are now available across the visible and near-infrared spectrum have enabled a diverse range of applications, from sensing [2–4], imaging [5,6], and LIDAR [7,8] to measurements of gravitational waves [9].

The terahertz region of the electromagnetic spectrum is comparatively underdeveloped, with a lack of stabilized laser sources. There are a number of applications where a narrow linewidth and stable terahertz source is essential. Remote sensing for atmospheric and astronomical observations makes use of local oscillators (LOs) [10–12] where the linewidth and stability of the LO source defines the resolution and accuracy of the measurement. A compact, stable, and narrow linewidth terahertz source is also highly desirable for satellite and airborne radiometry [13–15]. Furthermore, if terahertz laser sources could be stabilized with metrological precision, there are exciting applications in tests of physical constants [16–18] and charge conjugation parity [19] in this frequency region, where many gas molecules exhibit fundamental rotational and vibrational

modes. Recent advances in laser cooling have allowed molecules to be cooled to \sim mK and even \sim uK regimes [20], reducing the Doppler broadening of these molecular species to subkilohertz linewidths.

The most versatile and promising laser source in this part of the spectrum is the terahertz frequency quantum cascade laser (QCL). The appeal of this source has led to intense research activity in the field of terahertz QCLs since the first demonstration [21]. Major advances in the past decade include realization of emission frequencies ranging from 1.2 THz [22] to 5 THz [23], up to 2.4 W output power [24] and terahertz frequency comb emission [25]. The intrinsic linewidth of the terahertz QCL is of the order of a few hundreds of Hz [26,27] but thermal, electric, and mechanical instabilities typically result in free-running linewidths of a few MHz [28]. This has led to the development of several techniques to stabilize the frequency of QCLs, including locking to a gas absorption line [29], a multiplied microwave source [30], femtosecond laser frequency combs [31,32], and a femtosecond frequency comb stabilized to a primary frequency reference [33]. All of these methods only make use of an electrical feedback to stabilize the frequency of the QCL to a stable reference source. A significant drawback of this technique is that the bandwidth over which the frequency fluctuations can be compensated is limited

by the effective bandwidth of the negative feedback loop, usually around 1 MHz, limiting the proportion of the QCL signal that is locked, for example to 70% in Ref. [31]. Also, the relative phase between the QCL and the reference source is typically not well-defined when using only a negative feedback loop. Finally, previous work has not demonstrated phase-stable tunability of the locked frequency, a key requirement for spectroscopy applications.

In this work, we stabilize the frequency and the phase of a terahertz QCL by using terahertz injection locking (IL) combined with an electronic phase lock loop feedback configuration. The optical counterpart of this technique has already been demonstrated on a near-infrared laser in Ref. [34]. Our technique allows us to independently control the laser frequency and phase with very high precision, the first demonstration with a locked QCL. Furthermore, the combination of both locking schemes allows us to maintain lower phase error at low frequencies via the electronic PLL, while the addition of terahertz injection provides a wider locking range [34]. Hence, the combined implementation of the terahertz injection phase lock loop (IPLL) provides improved tracking of environmental fluctuations and low phase error variance compared to systems that use either IL [35] or only the electronic PLL configuration [29–32].

IL occurs when a stable “master” source is injected into an unstable “slave” source. The frequency of the locked slave source becomes exactly that of the injected master signal. The range of frequencies over which the slave laser is locked to the master is known as the locking range and depends on the injected power level [35]. While the output frequency of the slave source is exactly equal to that of the injected signal within the locking range, the phase difference between the slave and master varies by “ π ” across the locking range. We have previously used this technique to injection lock a 2.0 THz QCL [36]. Here, the addition of the PLL offers greatly improved locking characteristics as the frequency/phase fluctuations are compensated for over a wider bandwidth by both the terahertz IL and the electronic PLL paths. Furthermore, the combined locking configuration allows us to lock the QCL across the various phase points in the locking range, enabling precise control of the QCL emission phase independently without changing the QCL emission frequency, as will be discussed in Section 2.

The stable master frequency is provided by a near infrared (NIR) comb source with ~ 2.5 THz span [37] operating in the telecommunications “C” band (1530–1565 nm). The comb line spacing is determined exactly by a microwave synthesizer referenced to a rubidium frequency standard, whose frequency is locked by a Global Positioning System (GPS) receiver, enabling traceability to primary cesium frequency standards. By selecting two comb lines and heterodyning these on a photomixer, the high-precision microwave signal is multiplied to terahertz frequencies and used as the reference for the terahertz IPLL that, in turn, locks the QCL (see Supplement 1). Because measurements of the locked QCL linewidth typically rely on measuring the in-loop beat between the reference source and the QCL, the true line-shape of the locked QCL will only be revealed if the reference source stability is well known. Our comb source has a linewidth of < 101 Hz at 2 THz, several times less than Refs. [31–33] and comparable to the stability of a state-of-the-art femtosecond comb stabilized to atomic frequency standards [38] (see Supplement 1).

The experimental system is shown in Fig. 1. The comb source is driven by an RF synthesizer at a frequency f_{RF} that controls the spacing between the comb lines. This NIR comb is then filtered

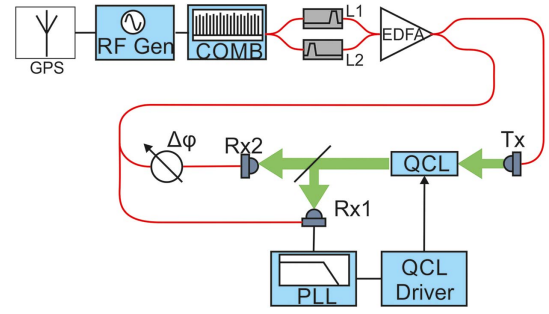


Fig. 1. Schematic diagram of the experimental arrangement. EDFA, erbium doped fibre amplifier; Tx, photomixer emitter; Rx1 and Rx2, photomixer receivers; PLL, phase lock loop; $\Delta\varphi$, variable delay line. Electrical connections are shown in black, optical fiber and IR connections in red, and terahertz connections in green.

and amplified to retain a pair of comb lines that have a frequency difference equal to $f_{\text{ref}} = N \times f_{\text{RF}}$, where N is the chosen number of comb line separations between the selected comb lines. In this case, $N = 101$, $f_{\text{RF}} = 19.7734$ GHz, and $f_{\text{ref}} = 1997.1134$ GHz. This NIR frequency difference is converted to the terahertz reference frequency by using a terahertz photomixer. The terahertz radiation from Tx is coupled into the terahertz QCL to injection lock the laser. Terahertz radiation from the QCL is then split and detected on the two photomixer receivers, Rx1 and Rx2. The signals are downconverted to low frequency by mixing with the same pair of NIR comb lines so that the terahertz electric field, E_{QCL} , is detected coherently and is proportional to the current detected from the photomixer [39]:

$$I_{\text{Rx1,2}} \propto E_{\text{QCL}} \sin[(f_{\text{ref}} - f_{\text{QCL}})t + (\varphi_{\text{ref}} - \varphi_{\text{QCL}})], \quad (1)$$

where f_{QCL} is the QCL frequency, φ_{ref} is the phase of the terahertz reference frequency, and φ_{QCL} is the phase of the terahertz QCL radiation. The terahertz signal from Rx1 is amplified and is used as the input signal for the phase lock loop (PLL). Rx2 is used to monitor the QCL output and has a variable delay path for the NIR reference so that the reference phase, φ_{ref} can be varied independently. Further details of the experimental arrangement can be found in the Supplement 1 and in Refs. [36,37].

2. RESULTS

The QCL was aligned for optimal coupling of the incoming terahertz radiation from the emitter at 2 THz. At an input IR power of 30 mW and a DC bias of -0.8 V, the CW terahertz power from the emitter at 1997 GHz was estimated to be ~ 100 nW. The QCL current was set to approximately 750 mA such that $(f_{\text{ref}} - f_{\text{QCL}}) \approx 0$ so that the QCL becomes injection locked to the terahertz reference frequency [36]. With the PLL switched off, the delay line is then scanned to record the terahertz field from the locked QCL on the lock-in amplifier, Fig. 2(a) (see Supplement 1). By changing the delay ($\Delta\varphi$) between the locked QCL and the reference frequency, we can control the detection phase. We can use this control to obtain different responses to frequency instability or modulation of the QCL. The expected signal at Rx2 for a locked QCL is [35,40],

$$I_{\text{Rx2}} \propto |E_{\text{QCL}}^L| \sin \left[\Delta\varphi + \sin^{-1} \left(\frac{f_{\text{ref}} - f_{\text{QCL}}^U}{f_{\text{lock}}} \right) \right], \quad (2)$$

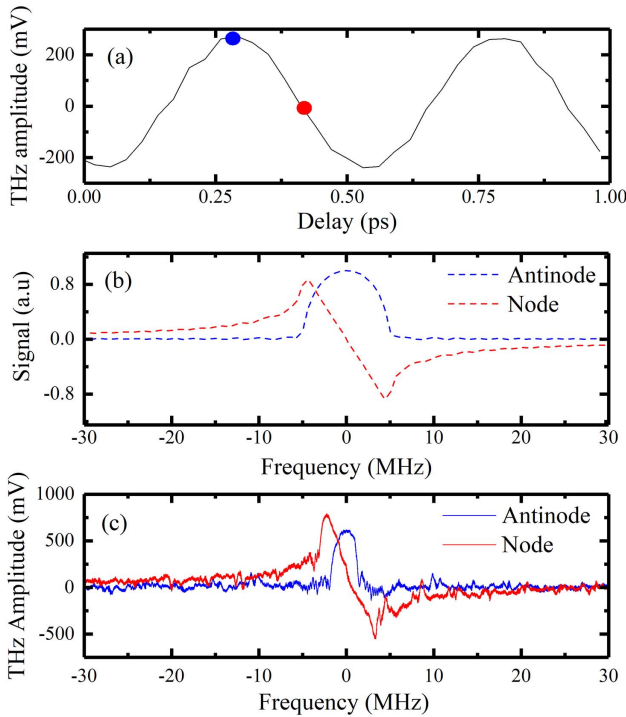


Fig. 2. (a) Terahertz electric field of the locked QCL at ~ 2 THz for $|f_{\text{ref}} - f_{\text{QCL}}| \approx 0$, as a function of delay. The node (red) and antinode (blue) positions are marked (b) calculated waveform shapes at the Rx2 for the node and antinode positions of the receiver and (c) terahertz amplitude from the Rx2 by modulating the QCL DC source at the node (red curve) and antinode (blue curve) positions of the Rx2 delay line. Frequency scale is the difference between the QCL frequency (tuned by the current modulation) and the terahertz reference frequency (constant).

where $|E_{\text{QCL}}^L|$ is the magnitude of the locked QCL signal, constant through the locking range, $\Delta\varphi$ is the phase difference added by the variable delay line, f_{QCL}^U is the underlying QCL frequency, and f_{lock} is the locking range. Outside the locking range the second term inside the sin function is $+\pi$ or $-\pi$ depending on sign of $(f_{\text{ref}} - f_{\text{QCL}})$. To demonstrate this, and with the PLL switched off, the QCL was modulated using a triangular wave at 2.5 kHz frequency. The QCL used for this experiment had a tuning sensitivity of -6.5 MHz/mA resulting in a modulation of the QCL emission frequency by 65 MHz for a modulation of 10 mA pk-pk. The signal detected at Rx2 is amplified with a transimpedance gain of $10^7 \Omega$ and measured using an oscilloscope. First, the detection phase is set to an antinode when $(f_{\text{ref}} - f_{\text{QCL}}) = 0$ [blue dot in Fig. 2(a)], corresponding to $\Delta\varphi = \pi/2$. As the underlying QCL frequency, f_{QCL}^U , is swept the blue curve in Fig. 2(c) is measured. As expected there is a peak in the signal when $(f_{\text{ref}} - f_{\text{QCL}}) \approx 0$, and toward the edges of the locking range the signal drops to zero because the phase between the QCL and the reference has changed by $\pi/2$, as expected [Eq. (2)].

Outside the locking range, the QCL and reference frequency beat at a frequency $f > f_{\text{lock}}$, which lies outside the detection bandwidth and therefore the signal drops to zero. An alternative approach is to set the detection phase to a node when $(f_{\text{ref}} - f_{\text{QCL}}) \approx 0$, indicated by the red dot in Fig. 2(a), corresponding to $\Delta\varphi = 0$. When the QCL frequency is now swept, the red curve in Fig. 2(c) is measured, showing the linear relationship between the frequency difference, $(f_{\text{ref}} - f_{\text{QCL}}^U)$, and the signal

on the receiver when within the locking range. Again, this is a consequence of the phase relationship predicted by Adler [35], shown in Eq. (2). This signal can be used as the input for the PLL to stabilize the phase of the QCL relative to the reference phase and also to ensure that the underlying QCL frequency remains within the locking range to ensure stability over longer time scales.

A. Terahertz IPLL

To achieve full stabilization, we make use of a PLL controller that provides feedback to the QCL bias current to control the underlying frequency, and hence the phase of the terahertz injection locked QCL, to form a terahertz IPLL as shown in Fig. 1 (further details in Supplement 1). Without any external modulation applied to the QCL, the QCL DC current is tuned to achieve a 0 V amplitude at Rx1 when the position of Rx1 is adjusted by changing the delay line to lie at the node for the center of the locking range ($\Delta\varphi = 0$). To form the terahertz IPLL, the output from Rx1 is connected to the input of the PLL electronics, and the PLL output is connected to the modulation control of the QCL current source. The QCL current is then controlled to compensate for drifts in the underlying QCL frequency, causing a phase shift, detected by Rx1. Since the terahertz reference frequency, f_{ref} , is stable, the major contributing factors to the drift in the QCL phase are the thermal fluctuations and mechanical vibrations. The slow thermal drift can be of the order of seconds and an integrating PLL filter is desirable; the PLL filter produces a feedback voltage proportional to the input voltage integrated over time.

To observe the effect of the terahertz IPLL, we monitor the terahertz spectrum of the locked QCL. Locking the QCL to the comb reduces the QCL linewidth to that of the injected terahertz reference signal. The locked QCL linewidth was measured for the terahertz-IL and terahertz-IPLL states by heterodyning the QCL terahertz signal with a replica of the terahertz reference frequency, f_{ref} , that has been shifted by 80.98 MHz using an acousto-optic modulator (AOM) (see Supplement 1 for details). The transimpedance amplifier gain and bandwidth for the Rx2 were adjusted to be $10^4 \Omega$ and 80 MHz, respectively, and the QCL spectrum measured by a low-noise spectrum analyzer. The accuracy of the measurement was improved by referencing the comb microwave synthesizer to a GPS-disciplined rubidium clock.

Figure 3 shows the measured linewidth spectra with spans of 10 kHz and 250 Hz for the terahertz IL (black curves) and terahertz IPLL (red curves). The beat note is centered at $f_s = 80.98$ MHz with the 3 dB linewidth measured to be < 1 Hz, which is the limit of our electrical spectrum analyzer. No change in linewidth was observed between the terahertz-IL and terahertz-IPLL states, confirming the narrow linewidth of the injected terahertz reference signal. However, additional sideband peaks are observed for the terahertz-IL state, with offset by $< \pm 50$ Hz from 80.98 MHz, attributed to the mechanical and thermal noises from the QCL. The terahertz-IPLL spectrum shows reduced low-frequency noise with only a small peak at $80.98 \text{ MHz} \pm 50 \text{ Hz}$ due to reduced phase error variance at low frequencies provided by the PLL [34]. When the terahertz radiation entering the detector is blocked, the peak signal measured on the spectrum analyzer drops by over 30 dB while the background noise level remains the same. By integrating the AOM data in Fig. 3, we calculate that at least 94% of the QCL power is phase locked for the terahertz-IPLL and at least 87% for the terahertz-IL [41]. These estimates are limited by the noise level for this measurement; however, when calculated from the noise

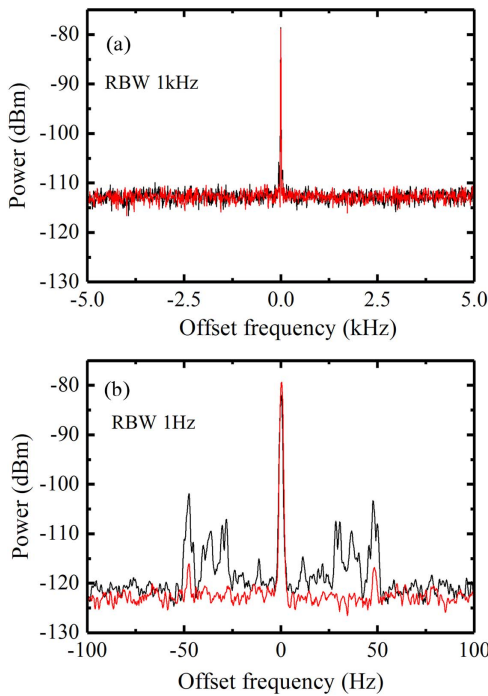


Fig. 3. Measured linewidth spectra for the terahertz-IL (black) and terahertz-IPLL (red) states. The resolution bandwidth (RBW) for each spectrum is indicated and the frequency is offset by 80.98 MHz for clarity. Spectra were acquired after 30 trace averages.

spectrum measured at low frequencies, we find 99% of the power is locked for the terahertz IPLL (see Supplement 1).

The stability of the terahertz-IPLL state can also be characterized over longer time scales by scanning the detection phase (delay) and extracting both the amplitude and phase of the terahertz electric field. This was done over a period of 10 min and is shown in Fig. 4 for both the terahertz-IL and terahertz-IPLL configurations. Care was taken to match the reference arm (to Rx2) length to the QCL arm and ensure that fibers were in close proximity to avoid temperature variations that could lead to phase instabilities. In the terahertz IPLL, the terahertz amplitude varies by $<3\%$. The terahertz QCL phase also remains stable, with deviation of $<5\%$ of the possible ' π ' range. Because the QCL remains locked to the reference frequency, the QCL frequency is stable throughout the measurement. For comparison, the stability of injection locked state, with the PLL switched off was also measured, shown as open symbols and dashed lines in Fig. 4. The amplitude drifts by more than 50% during the duration of the measurement. Correlated with the amplitude drift, the phase of the terahertz radiation also drifted, by a total of 0.5π . By the end of the measurement, the QCL in the terahertz-IL state was close to the edge of the locking range and only partially locked. The advantages of the terahertz-IPLL scheme over the simple terahertz-IL scheme are clear for applications where stability is required over long periods of time.

B. Frequency Tuning

Besides providing enhanced locking stability, the PLL can also be used to control both the phase and frequency of the QCL, as we demonstrate below. The frequency of the locked QCL is controlled by the injected reference frequency in both the terahertz-IL and terahertz-IPLL states. The frequency of the QCL can therefore

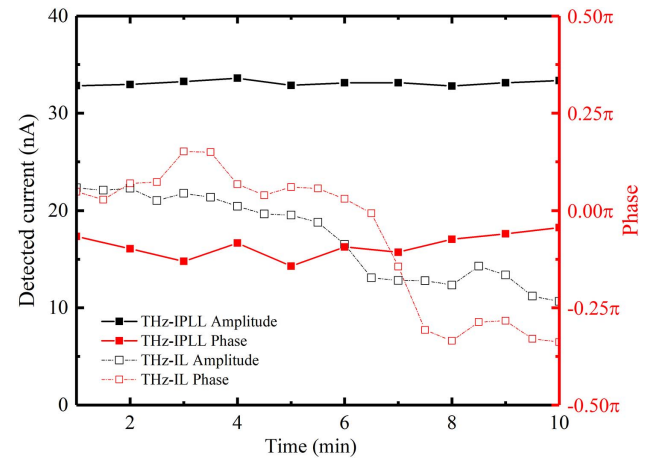


Fig. 4. Terahertz amplitude and phase at Rx2 measured as a function of time for the terahertz IL (hollow symbols with dotted lines) and terahertz IPLL (solid symbols with solid line). The delay line of the Rx2 was scanned for each data point for the same scan length, position, and resolution.

be adjusted by tuning the reference frequency, provided that the reference frequency remains in the locking range of the QCL. In practice, this means that for all but the smallest tunings (≤ 5 MHz), the underlying QCL frequency must also be tuned by controlling its drive current. The PLL used in the terahertz-IPLL scheme ensures that the QCL is tuned automatically so that the reference frequency always lies in the center of the locking range. The tuning range of the locked QCL is then limited only by the tuning range of the (unlocked) QCL cavity, 0.4 GHz for this device, but much larger electrical tunings are possible [42].

The terahertz reference frequency can be tuned by changing the RF synthesizer frequency, f_{RF} , which controls the comb spacing; $f_{ref} = f_{RF} \times 101$. While f_{ref} can be tuned across the full QCL tuning range of 400 MHz, the automated tuning range is limited to around 2 MHz by the need to manually adjust the optical delay line (loop length of the comb source) and the frequency of the digital supermode distributed Bragg reflector (DSDBR) lasers (see Supplement 1 for more detail). Figure 5 shows the change in QCL current and corresponding calculated change in QCL frequency, f_{QCL} , as the terahertz reference frequency, f_{ref} , is adjusted in discrete steps. The QCL current is monitored through the QCL power supply, which is under the control of the PLL. Tuning f_{RF} between 19.773515 GHz and 19.773525 GHz, a 10 kHz increase, changes f_{ref} from 1997.125015 GHz to 1997.126025 GHz, a 1.010 MHz increase in f_{ref} . This produces a reduction in QCL current of 0.16 mA, corresponding to an increase in the QCL frequency of 1.04 MHz, indicating that the QCL tracks the 1.01 MHz increase f_{ref} . The QCL remained in the locked state throughout the measurement, showing that the locked QCL can be tuned quickly and efficiently, with a resolution and precision limited only by f_{RF} .

C. Phase Control

While the locked QCL frequency is controlled by the injected reference frequency, the phase of the locked QCL (relative to the reference phase) can be controlled by adjusting the voltage at which we choose to stabilize the terahertz signal on Rx1; we are free to choose any point on the linear section of the red curve in Fig. 2(b).

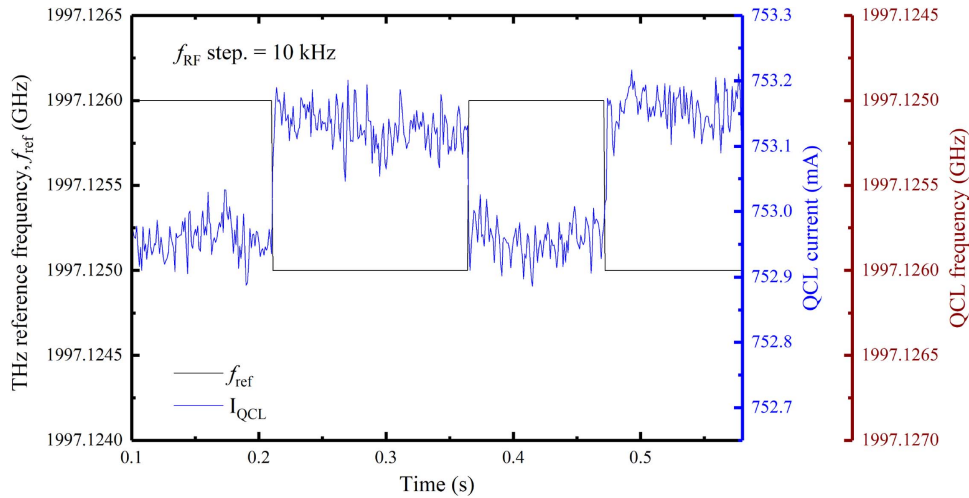


Fig. 5. QCL current, I_{QCL} , and QCL frequency, f_{QCL} , as a function of terahertz reference frequency, f_{ref} . The reference frequency is switched by 1010 kHz. The QCL frequency axis is calculated from the QCL current using measured tuning of -6.5 MHz/mA.

Up to this point, the offset voltage has been set to zero so that the QCL is stabilized to the center of the locking range and the QCL phase is identical to the reference phase. Now, we can set the offset voltage, or locking point for the PLL, to control the QCL phase while the frequency is controlled by the optical injection. In this way, it should be possible to access the full range of π phase values. Figure 6 shows the effect of adding a DC offset voltage to the PLL input (x axis). For each DC offset point, the electric field from the QCL is measured by scanning the delay line (shown as an inset to Fig. 6), and the amplitude and phase are extracted. The amplitude of the QCL electric field remains constant within $<3\%$ as the DC voltage offset was varied. This is expected because the change in QCL bias produced by the change in locking point is too small to have a significant change in the QCL power. The phase of the locked signal, however, changes from $+0.15\pi$ to -0.15π as the DC voltage offset is changed from -0.3 V to $+0.3$ V. This indicates that it is possible to control the phase in a range of $\sim 0.3\pi$ by adjusting the DC voltage, while the amplitude and frequency

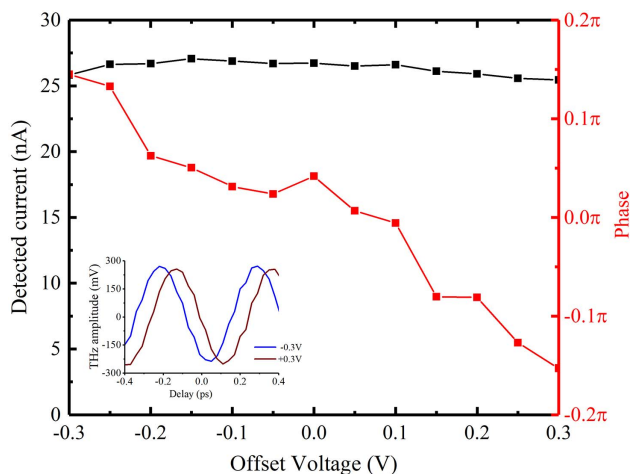


Fig. 6. Terahertz signal amplitude (black symbols and line) and phase (red symbols and line) plotted as a function of the DC voltage offset. The inset shows the phase change in the sinusoidal signal obtained by scanning the Rx2 for $+0.3$ V (blue) and -0.3 V (brown) values of the DC voltage offset. The delay line of Rx2 was scanned for each data point for the same scan length, position, and resolution.

of the laser remain fixed. Beyond the ± 0.3 V DC offset voltage the lock becomes unstable and the PLL filter amplifier became saturated.

3. CONCLUSIONS

The frequency and phase of a high-power terahertz frequency quantum cascade laser have been simultaneously locked to an IR frequency comb using a terahertz-IPLL scheme for the first time. The comb source is referenced to a microwave synthesizer locked to a rubidium standard locked by a GPS receiver, thereby linking the QCL frequency to primary frequency standards. The terahertz-IPLL scheme improved the locked QCL heterodyne linewidth to less than 1 Hz and improved the stability of the frequency and phase of the terahertz laser over extended timescales. Using this scheme, we also demonstrated independent, high-resolution, frequency and phase tuning of the terahertz laser. The frequency resolution is limited by the minimum frequency step size of the microwave source.

Such a tunable terahertz source that can be referenced to the primary frequency standards available in the microwave region is desirable for many applications, including high-precision terahertz gas spectroscopy and radiometry. Extended frequency coverage, limited only by the QCL tuning range, can be achieved by adjusting the delay within the comb loop [37]. The precise phase control of the terahertz source could find applications in terahertz phase modulation in phased array antennas in future terahertz communications [43]. Finally, we note that many of the components (IR comb, photomixers, QCL, and PLL) used in this work could be monolithically integrated into a single chip, making a compact and portable high-resolution terahertz system. The data associated with this paper is openly available from the University of Leeds data repository [44].

Funding. Engineering and Physical Sciences Research Council (EP/P021859/1).

Acknowledgment. We would like to acknowledge Dr. Viktor Doychinov from the School of Electronic and

Electrical Engineering, University of Leeds, Leeds, for providing the microwave synthesizer and electrical spectrum analyser, and Lumentum Technology, UK, for supplying the DSDBR lasers, customized for this experiment. This work was funded by the EPSRC programme grant ‘HyperTerahertz’ (EP/P021859/1). EHL acknowledges the Royal Society and the Wolfson Foundation.

Disclosures. The authors declare no conflicts of interest.

See [Supplement 1](#) for supporting content.

REFERENCES

1. T. H. Maiman, “Stimulated optical radiation in ruby,” *Nature* **187**, 493–494 (1960).
2. W. Zeller, L. Naehle, P. Fuchs, F. Gerschuetz, L. Hildebrandt, J. Koeth, W. Zeller, L. Naehle, P. Fuchs, F. Gerschuetz, L. Hildebrandt, and J. Koeth, “DFB lasers between 760 nm and 16 μm for sensing applications,” *Sensors* **10**, 2492–2510 (2010).
3. K. V. Pokazeev, A. S. Zapevalov, and K. E. Lebedev, “Measurements of sea surface slopes by laser sensing from a space vehicle,” *Moscow Univ. Phys. Bull.* **72**(4), 410–414 (2017).
4. J. G. Henning and P. J. Radtke, “Ground-based laser imaging for assessing three-dimensional forest canopy structure,” *Photogramm. Eng. Remote Sens.* **72**, 1349–1358 (2006).
5. B. Redding, M. A. Choma, and H. Cao, “Speckle-free laser imaging using random laser illumination,” *Nat. Photonics* **6**, 355–359 (2012).
6. X. Wang, Y. Pang, G. Ku, X. Xie, G. Stoica, and L. V. Wang, “Noninvasive laser-induced photoacoustic tomography for structural and functional in vivo imaging of the brain,” *Nat. Biotechnol.* **21**, 803–806 (2003).
7. D. N. Whiteman, S. H. Melfi, and R. A. Ferrare, “Raman lidar system for the measurement of water vapor and aerosols in the Earth’s atmosphere,” *Appl. Opt.* **31**, 3068–3082 (1992).
8. X. Dong, J. S. Fu, K. Huang, N. H. Lin, S. H. Wang, and C. E. Yang, “Analysis of the co-existence of long-range transport biomass burning and dust in the subtropical West Pacific Region,” *Sci. Rep.* **8**, 1–10 (2018).
9. B. P. Abbott, “Observation of gravitational waves from a binary black hole merger,” *Phys. Rev. Lett.* **116**, 61102–61116 (2016).
10. H. Richter, M. Wienold, L. Schrottke, K. Biermann, H. T. Grahn, and H. W. Hübers, “4.7-THz local oscillator for the GREAT heterodyne spectrometer on SOFIA,” *IEEE Trans. Terahertz Sci. Technol.* **5**, 539–545 (2015).
11. J. L. Kloosterman, D. J. Hayton, Y. Ren, T. Y. Kao, J. N. Hovenier, J. R. Gao, T. M. Klapwijk, Q. Hu, C. K. Walker, and J. L. Reno, “Hot electron bolometer heterodyne receiver with a 4.7-THz quantum cascade laser as a local oscillator,” *Appl. Phys. Lett.* **102**, 011123 (2013).
12. H. W. Hübers, “Terahertz heterodyne receivers,” *IEEE J. Sel. Top. Quantum Electron.* **14**, 378–391 (2008).
13. C. Risacher, R. Güsten, J. Stutzki, H.-W. Hübers, A. Bell, C. Buchbender, D. Büchel, T. Csengeri, U. U. Graf, S. Heyminck, R. D. Higgins, C. E. Honingh, K. Jacobs, B. Klein, Y. Okada, A. Parikka, P. Pütz, N. Reyes, O. Ricken, D. Riquelme, R. Simon, and H. Wiesemeyer, “The upGREAT 1.9 THz multi-pixel high resolution spectrometer for the SOFIA observatory,” *Astron. Astrophys.* **595**, A34 (2016).
14. Y. Ren, J. N. Hovenier, R. Higgins, J. R. Gao, T. M. Klapwijk, S. C. Shi, A. Bell, B. Klein, B. S. Williams, S. Kumar, Q. Hu, and J. L. Reno, “Terahertz heterodyne spectrometer using a quantum cascade laser,” *Appl. Phys. Lett.* **97**, 161103 (2010).
15. P. H. Siegel, “THz for space: the golden age,” in *IEEE MTT-S International Microwave Symposium* (2010), pp. 816–819.
16. C. Solaro, S. Meyer, K. Fisher, M. V. Depalatis, and M. Drewsen, “Direct frequency-comb-driven raman transitions in the terahertz range,” *Phys. Rev. Lett.* **120**, 253601 (2018).
17. E. R. Hudson, H. J. Lewandowski, B. C. Sawyer, and J. Ye, “Cold molecule spectroscopy for constraining the evolution of the fine structure constant,” *Phys. Rev. Lett.* **96**, 143004 (2006).
18. P. Jansen, H. L. Bethlem, and W. Ubachs, “Minimization of ion micromotion in a Paul trap,” *J. Chem. Phys.* **140**, 10901 (2014).
19. S. Albert, F. Arn, I. Bolotova, Z. Chen, C. Fábri, G. Grassi, P. Lerch, M. Quack, G. Seyfang, A. Wokaun, and D. Zindel, “Synchrotron-based highest resolution terahertz spectroscopy of the ν_{24} band system of 1,2-dithiine ($\text{C}_4\text{H}_4\text{S}_2$): a candidate for measuring the parity violating energy difference between enantiomers of chiral molecules,” *J. Phys. Chem. Lett.* **7**, 3847–3853 (2016).
20. N. Balakrishnan, “Perspective: ultracold molecules and the dawn of cold controlled chemistry,” *J. Chem. Phys.* **145**, 150901 (2016).
21. R. Kohler, A. Tredicucci, F. Beltram, H. E. Beere, E. H. Linfield, A. G. Davies, D. A. Ritchie, R. C. Iotti, and F. Rossi, “Terahertz semiconductor-heterostructure laser,” *Nature* **417**, 156–159 (2002).
22. C. Walther, M. Fischer, G. Scalari, R. Terazzi, N. Hoyler, and J. Faist, “Quantum cascade lasers operating from 1.2 THz to 1.6 THz,” *Appl. Phys. Lett.* **91**, 131122 (2007).
23. A. W. M. Lee, Q. Qin, S. Kumar, B. S. Williams, Q. Hu, and J. L. Reno, “Real-time terahertz imaging over a standoff distance (>25 meters),” *Appl. Phys. Lett.* **89**, 141125 (2006).
24. L. H. Li, L. Chen, J. R. Freeman, M. Salih, P. Dean, A. G. Davies, and E. H. Linfield, “Multi-watt high-power THz frequency quantum cascade lasers,” *Electron. Lett.* **53**, 799–800 (2017).
25. D. Burghoff, T.-Y. Kao, N. Han, C. Wang, I. Chan, X. Cai, Y. Yang, D. J. Hayton, J.-R. Gao, J. L. Reno, and Q. Hu, “Terahertz laser frequency combs,” *Nat. Photonics* **8**, 462–467 (2014).
26. M. S. Vitiello, L. Consolino, S. Bartalini, A. Taschin, A. Tredicucci, M. Inguscio, and P. De Natale, “Quantum-limited frequency fluctuations in a terahertz laser,” *Nat. Photonics* **6**, 525–528 (2012).
27. M. Ravaro, S. Barbieri, G. Santarelli, V. Jagtap, C. Manquest, C. Sirtori, S. P. Khanna, and E. H. Linfield, “Measurement of the intrinsic linewidth of terahertz quantum cascade lasers using a near-infrared frequency comb,” *Opt. Express* **20**, 25654–25661 (2012).
28. A. Barkan, F. K. Tittel, D. M. Mittleman, R. Dengler, P. H. Siegel, G. Scalari, L. Ajili, J. Faist, H. E. Beere, E. H. Linfield, A. G. Davies, and D. A. Ritchie, “Linewidth and tuning characteristics of terahertz quantum cascade lasers,” *Opt. Lett.* **29**, 575–577 (2004).
29. H. Richter, S. G. Pavlov, A. D. Semenov, L. Mahler, A. Tredicucci, H. E. Beere, D. A. Ritchie, and H.-W. Hübers, “Submegahertz frequency stabilization of a terahertz quantum cascade laser to a molecular absorption line,” *Appl. Phys. Lett.* **96**, 71112 (2010).
30. P. Khosropanah, A. Baryshev, W. Zhang, W. Jellema, J. N. Hovenier, J. R. Gao, T. M. Klapwijk, D. G. Paveliev, B. S. Williams, S. Kumar, Q. Hu, J. L. Reno, B. Klein, and J. L. Hesler, “Phase locking of a 2.7 THz quantum cascade laser to a microwave reference,” *Opt. Lett.* **34**, 2958–2960 (2009).
31. L. Consolino, A. Taschin, P. Bartolini, S. Bartalini, P. Cancio, A. Tredicucci, H. E. Beere, D. A. Ritchie, R. Torre, M. S. Vitiello, and P. De Natale, “Phase-locking to a free-space terahertz comb for metrological-grade terahertz lasers,” *Nat. Commun.* **3**, 1040–1045 (2012).
32. S. Barbieri, P. Gellie, G. Santarelli, L. Ding, W. Maineult, C. Sirtori, R. Colombelli, H. Beere, and D. Ritchie, “Phase-locking of a 2.7-THz quantum cascade laser to a mode-locked erbium-doped fibre laser,” *Nat. Photonics* **4**, 636–640 (2010).
33. S. Bartalini, L. Consolino, P. Cancio, P. De Natale, P. Bartolini, A. Taschin, M. De Pas, H. Beere, D. Ritchie, M. S. Vitiello, and R. Torre, “Frequency-comb-assisted terahertz quantum cascade laser spectroscopy,” *Phys. Rev. X* **4**, 21006 (2014).
34. R. T. Ramos, P. Gallion, D. Erasme, A. J. Seeds, and A. Bordonalli, “Optical injection locking and phase-lock loop combined systems,” *Opt. Lett.* **19**, 4–6 (1994).
35. R. Adler, “A study of locking phenomena in oscillators,” *Proc. IRE* **34**, 351–357 (1946).
36. J. R. Freeman, L. Ponnampalam, H. Shams, R. A. Mohandas, C. C. Renaud, P. Dean, L. Li, A. Giles Davies, A. J. Seeds, and E. H. Linfield, “Injection locking of a terahertz quantum cascade laser to a telecommunications wavelength frequency comb,” *Optica* **4**, 1059–1064 (2017).
37. L. Ponnampalam, M. Fice, H. Shams, C. Renaud, and A. Seeds, “Optical comb for generation of a continuously tunable coherent THz signal from 122.5 GHz to 27 THz,” *Opt. Lett.* **43**, 2507–2510 (2018).
38. D. Fehrenbacher, P. Sulzer, A. Liehl, T. Kälberer, C. Riek, D. V. Seletskiy, and A. Leitenstorfer, “Free-running performance and full control of a passively phase-stable Er: fiber frequency comb,” *Optica* **2**, 917–923 (2015).

39. I. S. Gregory, C. Baker, W. R. Tribe, I. V. Bradley, M. J. Evans, E. H. Linfield, G. Davies, and M. Missous, "Optimization of photomixers and antennas for continuous-wave terahertz emission," *IEEE J. Quantum Electron.* **41**, 717–728 (2005).
40. A. E. Siegman, *Lasers* (University Science books, 1989).
41. G. Santarelli, A. Clairon, S. N. Lea, and G. M. Tino, "Heterodyne optical phase-locking of extended-cavity semiconductor lasers at 9 GHz," *Opt. Commun.* **104**, 339–344 (1994).
42. I. Kundu, J. R. Freeman, P. Dean, L. Li, E. H. Linfield, and A. G. Davies, "Wideband electrically controlled vernier frequency tunable terahertz quantum cascade laser," *ACS Photon.* **7**, 765–773 (2020).
43. H.-T. Chen, W. J. Padilla, M. J. Cich, A. K. Azad, R. D. Averitt, and A. J. Taylor, "A metamaterial solid-state terahertz phase modulator," *Nat. Photonics* **3**, 148–151 (2009).
44. R. A. Mohandas, L. Ponnampalam, L. Li, P. Dean, A. J. Seeds, E. H. Linfield, A. Giles, and J. R. Freeman, "Dataset for exact frequency and phase control of a terahertz laser," Research Data Leeds Repository (2020), <https://doi.org/10.5518/705>.